Surface modification of thin-film composite forward osmosis membranes with polyvinyl alcohol–graphene oxide composite hydrogels for antifouling properties

Nawshad Akther[a], Syed Muztuza Ali[a], Sherub Phuntsho[a] and Hokyong Shon[a]*

[a] School of Civil and Environmental Engineering, University of Technology Sydney (UTS), NSW 2007, Australia

* Corresponding author: Prof. Hokyong Shon Email: hokyong.shon-1@uts.edu.au; Tel.: +61 2 9514 2629; Fax: +61 2 9514 2633.

Abstract

In this study, the polyamide (PA) layers of commercial thin-film composite (TFC) forward osmosis (FO) membranes were coated with glutaraldehyde cross-linked polyvinyl alcohol (PVA) hydrogel comprising of graphene oxide (GO) at various loadings to enhance their fouling resistance. The optimal GO concentration of 0.02 wt% in hydrogel solution was confirmed from the FO membrane performance, and its influence on membrane antifouling properties was studied. The properties of the modified membranes, such as surface morphology, surface charge and wettability, were also investigated. PVA/GO coating was observed to increase the smoothness and hydrophilicity of the membrane surface. The foulant resistances of the pristine, PVA-coated and PVA/GO-coated membranes were also reported. PVA hydrogel-coated TFC membrane with a GO loading of 0.02 wt% showed a 55% reduction in specific reverse solute flux, only a marginal reduction in the water flux, and the best antifouling property with a 58% higher flux recovery than the pristine TFC membrane. The significant improvement in the selectivity of the modified membranes meant that the hydrogel coating could be used to seal PA defects. The biocidal GO flakes in PVA hydrogel coating also improved the biofouling resistance of the modified membranes, which could be attributed to their morphologies and superior surface properties.

1 Introduction

Water pollution from the discharge of large quantities of contaminants produced from human activities is one of the primary reasons for making water shortage a severe global problem. Consequently, treatment and safe reclamation of industrial and municipal wastewater are necessary as a sustainable solution to meet the growing freshwater demand, and protect the human health and environment from harmful pollutants [1]. Stringent water guidelines and the need to treat wastewater with robust, energy-efficient and low-cost methods that require minimal chemicals have made membrane technology popular for wastewater reclamation and reuse [2-4]. Pressure-driven membrane processes, such as nanofiltration (NF) and reverse osmosis (RO), have been studied for high-quality clean water production [2]. Nonetheless, the efficiency of these processes is hampered with complex feed types that increase membrane fouling propensity and consequently lead to high energy consumption.

Forward osmosis (FO) process, on the other hand, uses the osmotic pressure difference between the feed solution (FS) and draw solution (DS), rather than the hydraulic pressure, to transport water molecules from FS to DS across a selective membrane [5, 6]. Fouling in FO processes is more reversible than pressure-driven processes due to the absence of hydraulic pressure, thus, forming a less compact organic fouling layer that can be removed by simple backwashing and flushing. Hence, membrane cleaning in FO is much simpler than the pressure-driven processes without significant requirement of chemical cleaning [6-8]. Therefore, FO membranes have been extensively researched for application in osmotic membrane bioreactor (OMBR) for wastewater treatment and reuse [9]; and can produce high-quality water by rejecting pathogens, particles and total dissolved solids (TDS).

57   Additionally, FO processes are more energy-efficient than RO when DS recovery is not

58   required. For instance, they can be used for fertigation [10], treating wastewater [9], dewatering

59   sludge [11] and concentrating juice [12] without needing DS recovery. Moreover, FO can be

60   implemented in hybrid systems for treating highly saline feeds that cannot be treated by RO [13,

61   14], and is suitable for directly pretreating complex feed and wastewaters [15]. Consequently, it is

62   essential to develop highly selective FO membranes with excellent antifouling properties, which

63   will not only reduce the use of chemical cleaning reagents and maintenance costs but will also

64   increase the membrane lifetime and offer consistent membrane performance.

65   The thin-film composite (TFC) membranes are most widely used for FO applications, and

66   they comprise of a thin polyamide (PA) selective layer supported on a highly porous substrate.

67   Both the selectivity and antifouling properties of the TFC membranes are primarily governed by

68   the membrane selective layer properties [16]. For example, a smoother membrane surface can

69   minimise foulant accumulation within the ridge-and-valley structures of the PA active layer [17].

70   Whereas, a hydrophilic surface can prevent adsorption of hydrophobic foulants by creating a water

71   layer barrier between the foulants and the hydrophilic active layer [18]. Consequently, several

72   strategies like nanomaterial addition and polymer coating on the membrane active layer have been

73   examined to enhance the antifouling properties of the membranes [19-21]. Gao's group grafted

74   polyvinyl alcohol (PVA) on PA TFC membrane to obtain chlorine resistant and antifouling

75   membranes [22]. The hydrophilic PVA layer acted as a protective barrier to hinder chlorine attack

76   on PA chain and minimised adsorption of hydrophobic foulants on the membrane surface. Zhang

77   et al. also reported similar results by optimising the process conditions of PVA film coating on PA

78   TFC RO membranes. The optimal membrane demonstrated improved solute rejection and good

79   antifouling properties towards dodecyl trimethyl ammonium bromide [23].

4

80   Graphene oxide (GO) has gained a lot of attention for its inherent hydrophilicity and biocidal

81   properties, and has been used as a filler to enhance membrane properties for several applications

82   like desalination and wastewater treatment [19, 21, 24-26]. Hegab et al. coated GO flakes on the

83   surface of PA TFC FO membranes using the bioadhesive polydopamine (pDA) facilitated

84   immobilisation method. The GO-modified membrane achieved 80% and 22% improvement in

85   selectivity and water flux, respectively, in addition to demonstrating significant anti-biofouling

86   properties compared to the pristine membrane [27]. Yin et al., on the other hand, embedded

87   multilayer GO flake structure with an interlayer spacing of ~ 0.83 nm into the PA layer of the thin-

88   film nanocomposite (TFN) membranes during the interfacial polymerisation (IP) reaction [28].

89   Results indicated that, in comparison to the pristine membrane, addition of 0.015 wt% of GO flakes

90   in the organic phase during IP process improved the permeate flux by 52% while slightly reducing

91   the sodium chloride (NaCl) rejection by 2% under 300 psi. The improvement in water permeability

92   was attributed to the GO interlayer spacing that may have worked as water channels.

93   Owing to the desirable properties of both PVA and GO flakes as membrane coating, this

94   work sought to systematically explore the influence of cross-linked hydrophilic PVA hydrogel and

95   GO flake composite coating on the physicochemical properties, selectivity and antifouling

96   properties of commercially-available TFC PA FO membranes. The PVA/GO hydrogel was coated

97   on TFC membranes using a simple dip-coating method. For the first time, this study shows a facile

98   and efficient method to improve the performance and antifouling properties of commercial FO

99   membrane by benefiting from the synergistic effects of intrinsically antifouling GO-modified PVA

100   hydrogel coating, which could increase the effectiveness of TFC FO membranes in wastewater

101   treatment.

2   Materials and methods

2.1   Chemicals

Commercially available PA TFC FO flat-sheet membranes from Toray Industries were used for surface modification in this study. PVA (96% hydrolysed, average MW 85,000–124,000 g/mol), sodium alginate (SA, low viscosity), calcium chloride dihydrate ($\geq$ 99%) and glutaraldehyde solution (GA, grade II, 25% in water) were procured from Sigma Aldrich. Sulfuric acid (H_2SO_4, 98%) and sodium chloride (NaCl, > 99.7%) were supplied by RCI Labscan Ltd and Chem Supply, respectively. Monolayer GO with particle size less than 10 μm was obtained from Graphenea (4 mg/mL dispersion in water). Deionised water (DI, Milli-Q) with a resistivity of approximately 18 MΩ/cm was used for FS and DS preparation. All reagents purchased were of analytical grade and used as received.

2.2   Hydrogel preparation and coating on PA TFC membrane

The PVA hydrogel solution was prepared using a previously reported method [29]. Briefly, PVA crystalline powder was added to DI water at 90 °C and dissolved by stirring for 8 h to obtain 0.25 wt% PVA aqueous solution. After cooling the PVA solution to room temperature, GA and 2 M H_2SO_4 were added simultaneously as a cross-linking agent and catalyst, respectively, under vigorous stirring for 15 min at 60 °C to prepare hydrogel solution. The catalyst concentration was adjusted to 1 wt% of the hydrogel solution; whereas, the GA weight was determined using Eq. 1 to achieve a theoretical cross-linking degree of 30%:

$$\chi_{CL}(\%) = 2\left(\frac{MW_{PVA\,unit}W_{CL}}{W_{PVA}MW_{CL}}\right)100\% \qquad (1)$$

121 where χ_{CL}, $MW_{PVA\,unit}$, W_{CL}, W_{PVA} and MW_{CL} denote the theoretical cross-linking degree,

122 molecular weight of one PVA unit, weight of cross-linking agent, weight of PVA, and molecular

123 weight of the cross-linking agent, respectively.

124 PVA hydrogel solutions with various GO loadings (0.01, 0.02 and 0.04 wt/v%) were

125 prepared using the same protocol as above except for the addition of GO to PVA aqueous solution

126 at room temperature followed by stirring and sonication for 30 min each. GA and catalyst were

127 then added to the PVA/GO aqueous solutions to prepare the PVA/GO composite hydrogel

128 solutions. The starting GO concentration was chosen as 0.01 wt/v% as it was found to be the

129 optimal GO concentration in our previous study [30].

130 The hydrogel was coated on the PA TFC FO membrane by first fixing the membrane in a
131 rectangular frame with the PA layer exposed for coating. The exposed PA membrane surface
132 was then immersed in the hydrogel solution for 4 min. Next, the surplus hydrogel solution was
133 poured out from the membrane surface, and any remaining solution was gently removed using an
134 air knife. The hydrogel coated membranes were later cured in an oven at 60 °C for 10 min.
135 Finally, the membranes were rinsed with DI water to eradicate the unreacted PVA molecules and
136 stored in DI water at 4 °C.

137   presents the surface modification conditions and the abbreviation of the various membranes

138   prepared in this study.

139

2.3 Membrane characterisation

Fourier transform infrared spectra (FTIR, Shimadzu MIRacle 10ATR-FTIR) of the membrane samples was analysed to confirm the PVA hydrogel grafting and GO flake integration on the membrane surface. All membrane samples were dried under ambient conditions before analysis. Scanning electron microscope (SEM, Zeiss Supra 55VP) was utilised to investigate the morphology of the PVA-coated membrane surface. The dry membrane samples were fixed on stubs with copper tape followed by sputter-coating with a gold layer at a thickness of 8 nm before SEM analysis. Atomic force microscopy (AFM, Dimension 3100, Bruker) was employed in tapping mode to determine the membrane surface roughness. The contact angles on the membrane surfaces were measured at ambient conditions with Attension Theta Lite 100 optical tensiometer from Biolin Scientific to ascertain the membrane hydrophilicity. At least seven measurements were made randomly for each membrane sample, and the average contact angle was reported. The membrane surface zeta potential was assessed via electrokinetic analyser (SurPASS^{TM} 3, Anton Paar). The membrane samples were fixed to the holder with a gap height of ~100 µm. Zeta-potentials were determined using a 1 mM KCl electrolyte solution over a pH range of 3 to 10, which was adjusted with 0.05 M NaOH and HCl solutions by an automated titration system.

2.4 Membrane performance assessment

A laboratory-scale FO experimental setup, as described in our previous work [16], was used to determine the performance of membrane samples with an effective area of 20 cm^2. The FO cell used for testing the membranes had a 3 mm deep flow channel on each side of the membrane. The co-current flow rate of both the FS and DS was maintained at 0.5 L/min (12.6 cm/s) at 22 °C,

9

161   unless otherwise stated, during the FO membrane performance tests. The membranes were tested

162   in AL-FS (active layer facing the feed solution) orientation with 1 M NaCl and DI water used as

163   DS and FS, respectively. The membrane water flux (J_w, L.m^{-2}.h^{-1}) was determined from the weight

164   of FS, which was automatically logged at constant time interval by a digital weight balance (Eq.

165   S1). The reverse solute flux (J_s, g.m^{-2}.h^{-1}) through the membrane was calculated by monitoring the

166   FS salinity using a conductivity meter (Eq. S2). The specific reverse solute flux (*SRSF*, g/L) for

167   all membranes was calculated from water and reverse solute flux values to indicate the membrane

168   selectivity (Eq. S3). All the equations used for calculating the membrane performance parameters

169   are provided in Section S1 of the Supporting Information (SI).

170   The pure water permeability coefficient (A), solute permeability coefficient (B) and intrinsic

171   selectivity (B/A) of the membranes were evaluated with the 4-stages non-linear regression model

172   developed by Tiraferri et al. [31] for FO membranes as explained in our previous study [30]. The

173   water and reverse solute fluxes of the FO membranes were determined at the four different NaCl

174   DS concentrations (0.5, 1, 1.5 and 2) using the same experimental conditions as the FO

175   performance tests. The average FO performance results of at least three samples from each

176   membrane type was used to acquire the intrinsic transport parameters.

177   **2.5   Membrane fouling test**

178   The FO membrane fouling experiments were conducted in AL-FS orientation with the same

179   protocol used in our previous work [30]. Firstly, the FO test was conducted for 1 h at a flow rate

180   of 0.5 L/min to set the initial baseline water flux ($J_{w,0}$) for each membrane at ~22 L.m^{-2}.h^{-1} by

181   adjusting the DS concentration between 0.5 M and 1 M. Secondly, a fouling study was performed

182   for 5 h at a flow rate of 0.5 L/min by adding 1 mM calcium chloride and 200 ppm SA as foulants

10

183   to the FS. The DS concentration was maintained throughout the fouling test to prevent flux decline

184   from DS dilution effect. Thirdly, the membranes were cleaned for 1 h after the fouling tests by

185   circulating DI water at an increased flow rate of 0.7 L/min in both DS and FS channels without

186   using any chemical reagents. Finally, the cleaned membranes were tested with the baseline

187   conditions to determine the flux recovery.

2.6   Foulant resistance evaluation

189   The transient foulant resistances of the pristine and hydrogel-coated FO membranes were

190   attained using the detailed procedure described by Siddiqui et al. [32]. Foulant resistance was

191   reported to describe the membrane fouling behaviour more accurately compared to the typical

192   permeate flux decline method. This is because the proposed method takes into account the foulant

193   accumulation effect and the internal concentration polarisation self-compensation effect. The

194   foulant resistance (R_f) was determined using Eq. 2:

$$R(m^{-1}) = R_m + R_f = \frac{F}{\mu J_w} \tag{2}$$

195   where F is the osmotic driving force across the membrane, μ denotes the solution viscosity, J_w

196   represents the water flux, and R is the overall hydraulic resistance against the water permeation

197   obtained by adding the membrane resistance (R_m) and foulant resistance (R_f). Detailed

198   information on the evaluation of foulant resistance for the fouled membranes is provided in Section

199   S3 of the SI.

2.7   Static bacterial adhesion test

201   Static bacterial adhesion tests were conducted using gram-positive *Bacillus subtilis* as model

202   bacteria to examine the anti-biofouling properties of the membranes. First, the bacteria were

203   inoculated in tryptic soy broth (TSB) medium from a single *Bacillus subtilis* colony by shaking at

204   120 rpm for 18 h at 37 °C. Second, the TSB medium was used to dilute the bacterial suspension

205   50 times prior to culturing it for 4 h at 30 °C. TSB medium was used again to adjust the bacterial

206   suspension to acquire an optical density of 0.05 at a wavelength of 450 nm with a

207   spectrophotometer (V-650, Jasco, Japan). Third, membranes (0.5 cm × 3 cm) were immersed in

208   the bacterial suspension for 24 h at 30 °C to determine the bacterial growth. The soaked membranes

209   were then rinsed twice with 0.85 wt% NaCl solution to remove weakly attached bacteria. Fourth,

210   a NaCl solution (0.85 wt%) with SYTO9 (Life Technologies Corporation, Carlsbad, CA) was used

211   to stain the adhered bacteria on the membrane surface for 20 min. A GA solution (2.5 wt%) was

212   then used for 2 min to fix the stained bacteria on the membrane surface. Lastly, the membrane

213   samples were examined by confocal laser scanning microscopy (CLSM; FV1000D, Olympus,

214   Japan) and the obtained images were studied by ImageJ software (National Institutes of Health,

215   USA) to quantify bacterial coverage.

3   Results and discussion

3.1   Membrane characterisation

218   In this study, the active layers of commercial PA TFC FO membranes were coated with GA

219   cross-linked PVA hydrogels containing different concentrations of GO flakes to improve the

220   antifouling properties of the membrane. To verify the existence of hydrogel coating on the

221   membrane surfaces, the surface chemistry of the pristine, PVA-coated and PVA/GO-coated TFC

222 membranes were examined from the ATR-FTIR spectra as presented in **Fig. 1**. The full ATR-FTIR

223 spectra of the pristine and modified TFC membranes show the typical peaks associated with the

224 polysulfone (PSf) support layer and thin PA active layer. The characteristic strong peaks at 1502

225 cm^{-1}, 1385 cm^{-1} and 1236 cm^{-1} relate to the C=C in-plane aromatic ring bend stretching vibration,

226 symmetric C–H deformation of $C(CH_3)_2$, and asymmetric C–O–C stretching vibration of the aryl–

227 O–aryl group; whereas, the peaks at 1292 cm^{-1} and 1147 cm^{-1} represent the asymmetric and

228 symmetric stretching vibrations of the O=S=O bonds found in PSf, respectively [33, 34].

229 The spectra for all the membranes demonstrate the characteristic peaks of PA at 1668 cm^{-1}

230 and 1606 cm^{-1}, which are attributed to the amide I and the aromatic amide band, respectively. The

231 pristine TFC membrane also reveals a peak at 1541 cm^{-1} conforming to the C–N stretching and

232 N–H in-plane bending vibration of the amide group in PA (amide II band), which splits into two

233 peaks at 1545 cm^{-1} and 1538 cm^{-1} for the pristine PVA-coated (TFC–P) and PVA/GO-coated

234 (TFC–PGO) TFC membranes due to the reaction between GA's aldehyde groups and PA's amide

235 bonds (–CO–NH–) [34, 35]. Additionally, the relative peak intensities at 1651 cm^{-1}, ascribed to

236 the C=N stretching, increased for the modified membranes due to the reaction between the end

237 amino groups of the PA and the aldehyde groups of GA [35]. The peak at 1737 cm^{-1} is ascribed

238 to the ester group (O=C–O) present in the PVA coating on the membrane surface, and the residual

239 aldehyde groups of GA that remained unreacted during the acetalisation cross-linking reaction [35,

240 36]. The presence of a new peak at 1024 cm^{-1} on the spectra of the modified membranes indicates

241 the formation of ether group (C–O–C) during the reaction between the hydroxyl and aldehyde

242 group of PVA and GA, respectively [37].

243   The relative intensities of peaks at 2920 cm^{-1} and 2850 cm^{-1} assigned to the C–H asymmetric

244   and symmetric stretching vibration, respectively, are weaker for TFC–P than the TFC membrane

245   because of the dilution effect of the PVA coating layer. On the contrary, TFC–PGO shows more

246   intense peaks at 2920 cm^{-1} and 2850 cm^{-1} than the TFC–P membrane due to the asymmetric and

247   symmetric stretch of C–H bonds in GO flakes [30]. The broad peak from 3100 to 3700 cm^{-1} results

248   from the coinciding peaks that are attributed to the carboxyl group and N–H stretching of the PA,

249   and hydroxyl groups (O–H) stretching of the PVA and GO flakes. Consequently, the peak

250   intensity at 3357 cm^{-1} is the highest for the TFC–PGO membrane due to the presence of abundant

251   O–H groups in both GO flakes and cross-linked PVA. Overall, the results of ATR-FTIR analysis

252   validate the effective coating of GA cross-linked PVA on the PA layer surface and the GO flakes

253   integration into the PVA hydrogel coating.

254   The morphologies of the pristine and modified TFC membrane surfaces were examined from

255   the SEM (**Fig. 2**) and AFM (**Fig. 3**) micrographs that clearly show the changes in membrane

256   morphologies following the surface modification. The SEM images show a uniform distribution

257   of the typical ridge-and-valley PA formations on the pristine TFC membrane surface (**Fig. 3**a);

258   however, more distinct physical irregularities can be observed for the modified membranes (**Fig.**

259   **3**b-e). Coating the PA layer with cross-linked PVA (TFC–P), as shown in Fig. 3b made the TFC

260   membrane surface denser and considerably smoother than the pristine TFC membrane. However,

261   the surfaces of the PVA-coated TFC membranes became more inconsistent after incorporating GO

262   flakes, forming patches that eventually covered the PA protrusions completely at a GO loading of

263   0.04 wt% (Fig. 3e).

264   The membrane surface roughness was quantitatively characterised using AFM (**Fig. 3**). The

265   average (R_a), maximum (R_{max}) and root mean square values (R_q) of the membrane surface

266   roughness are provided in Table S1. The R_q values of the pristine TFC membrane and modified

267   TFC–P, TFC–PGO1, TFC–PGO2 and TFC–PGO4 were found to be 42.0 nm, 29.8 nm, 38.0 nm,

268   34.2 nm and 28.8 nm, respectively. The membrane roughness decreased after coating the TFC

269   membrane surface with PVA hydrogel (**Fig. 3**b). However, the roughness of the modified

270   membranes increased after the addition of GO flakes in the PVA hydrogel, which eventually

271   decreased with an increase in GO loading (**Fig. 3**c-e). It can be seen from both the SEM and AFM

272   images that PVA hydrogel without GO flakes uniformly coated the membrane surface. On the

273   contrary, the addition of GO flakes in PVA hydrogel formed irregular patches of PVA hydrogel

274   aggregates on the membrane surfaces. A GO loading of 0.01 wt% formed smaller hydrogel

275   aggregates resulting in rougher membrane surface; whereas, the highest GO loading of 0.04 wt%

276   formed large hydrogel aggregates that completely covered the membrane surface to provide the

277   smoothest surface. The changes in membrane morphology could occur from the interaction

278   between GO and PVA, where the non-uniform coating may most likely result from the

279   solidification of PVA hydrogel directly on top of the GO flakes instead of the PA layer itself.

280   Overall, the coated membranes were much smoother than the pristine TFC membranes because of

281   the preferential deposition of PVA over the valley regions of the PA layer, which may improve

282   the antifouling property of the membranes by reducing the surface area for foulant adhesion [38].

283   The wettability of membrane surfaces before and after surface modification was determined

284   from water contact angle measurements made at the air-water interface. As presented in **Fig. 4**a,

285   the average water contact angle on the membrane surface significantly reduced from 96.9° for the

286   pristine TFC membrane to 79.5°, 75.9°, 74.7° and 69.0° for the hydrogel-coated membranes TFC–

15

287   P, TFC–PGO1, TFC–PGO2 and TFC–PGO4, respectively, which confirms the enhancement in

288   membrane hydrophilicity after surface modification. The improved hydrophilicity of the modified

289   membranes could be ascribed to the hydrophilic nature of PVA and GO flakes arising from the

290   presence of oxygen-containing functional groups. Membrane surface hydrophilicity is critical as

291   it can significantly affect membrane performance. Increased membrane surface wettability could

292   not only assist towards improving water permeation, but also reduce adsorption of hydrophobic

293   foulants on membrane surfaces by creating a water barrier between the hydrophilic membrane

294   surface and the hydrophobic foulants [39].

295   The surface charges of the pristine and modified membranes were determined by measuring

296   their surface zeta potentials over a pH range of 3 to 10. As can be observed from **Fig. 4**b, all

297   membrane surfaces were negatively-charged at pH higher than 3.8 due to the deprotonation of the

298   amino and carboxyl functional groups of the PA layer [40]. Besides, the increasing surface

299   negative charge of all the membranes at higher pH could be attributed to the adsorption of chloride

300   ions from the electrolyte solution on membrane surface [30]. At lower pH, the membranes revealed

301   positively-charged surfaces because of the protonation of the PA end amino groups. The pristine

302   TFC membrane was the most negatively-charged due to the existence of abundant carboxyl groups.

303   The modified TFC membranes, on the other hand, demonstrated lower surface negative charge

304   than the pristine TFC membrane because the shielding effect of the hydrogel coating on membrane

305   surface diminished the exposure of PA carboxyl groups [22]. These results are expected due to the

306   neutral properties of the PVA molecules. Finally, the zeta potential of the PVA/GO-coated

307   membranes was higher than the pristine TFC membrane, but lower than the PVA-coated (TFC-P)

308   membrane. The surface negative charge of PVA/GO-coated membranes increased with an increase

309   in GO loading because GO flakes contain abundant oxygen-containing functional groups, such as

310   the carboxyl groups, that increase negative charges by deprotonating at alkaline conditions. **Fig.**

311   **4**b also reveals the isoelectric point (IEP), where the membrane surface carries no net charge. The

312   IEPs of the modified membranes move to lower pH after incorporating GO flakes in the PVA

313   hydrogel due to the increasing amount of acidic functional groups from GO [30, 41].

314   Overall, the changes in membrane surface chemistry, morphology, wettability and charge

315   after modification confirm the successful coating of the cross-linked PVA and GO on the PA layer

316   of the commercial TFC FO membrane. The above characterisation results also established that the

317   physicochemical properties of the PVA-coated membranes could be adjusted by changing the GO

318   loading in PVA hydrogel.

319   **3.2   Membrane performance evaluation**

320   The FO membrane performance including the water flux, reverse solute flux and *SRSF* were

321   evaluated for the pristine and modified membranes in AL-FS orientation using DI water as FS and

322   1 M NaCl as DS (**Fig. 5**). As expected, the modified membranes demonstrated lower water and

323   reverse solute flux than the pristine TFC membranes as a result of the increased hydraulic

324   resistance from the PVA or PVA/GO cross-linked hydrogel layer that impeded water permeation.

325   While the PVA coating improved the membrane surface wettability, which is essential to promote

326   water permeability, the reduction in water flux occurred as the negative effect of additional

327   hydraulic resistance transcends the positive influence of increased hydrophilicity. The dense PVA

328   or PVA/GO coating improved the TFC membrane selectivity by augmenting the effect of size

329   exclusion to draw solute; thus, decreasing the reverse solute flux across the modified membranes.

330   Conversely, the water flux through the modified membranes increased after GO flake

331   addition up to a loading of 0.02 wt% (TFC–PGO2), while retaining membrane selectivity. Both

332   the water flux and reverse solute flux were observed to decrease on further increasing the GO

333   loading to 0.04 wt%. The higher water flux of TFC–PGO1 and TFC–PGO2 compared to the TFC–

334   P could be ascribed to their reduced hydraulic resistance owing to more PA surface exposure from

335   the uneven PVA coating on their surfaces as discussed earlier (**Fig. 3**b-d). Additionally, the

336   improved hydrophilicity of the TFC–PGO1 and TFC–PGO2 could have also contributed to the

337   enhancement in their water flux than the TFC-P membrane. The rougher membrane surfaces and

338   the slight increase in the reverse solute flux of the TFC–PGO1 and TFC–PGO2 than the TFC–P

339   membrane further confirmed that the discontinuous PVA/GO coating contributed to their water

340   flux enhancement. The TFC–PGO4 demonstrated a significant decline in both the water and

341   reverse solute flux due to the creation of a very dense hydrogel layer that covered almost the entire

342   PA surface as evident from its smoother surface (Fig. 3e) compared to that of the TFC–P

343   membrane (Fig. 3b). The nonporous GO flakes at a loading of 0.04 wt% also created impervious

344   regions in PVA hydrogel matrix, which could have inhibited both water and solute permeation

345   across the TFC membrane [42]. Consequently, the TFC–PGO4 demonstrated the lowest water flux

346   (18.0 L.m^{-2}.h^{-}1) and reverse solute flux (2.7 g.m^{-2}.h^{-1}) compared to the other modified membranes.

347   Besides, the high concentration of GO flakes in the PVA hydrogel could increase the composite

348   hydrogel layer's tortuosity by forming numerous water channels at the GO-PVA interface [43].

349   The SRSF is an essential parameter for evaluating the FO membrane selectivity, where a

350   more selective membrane exhibits a smaller SRSF value. The modified membranes exhibited at

351   least 56% lower SRSF than the pristine TFC membrane due to the dense PVA or PVA/GO layer

352   formation. The pristine TFC membrane showed the highest SRSF value (0.47 g/L) because of the

353   looser dynamic pore structure of the PA layer that allowed comparatively more solute to diffuse

354   from the DS to the FS. The SRSF values of TFC–P (0.19 g/L), TFC–PGO1 (0.22 g/L) and TFC–

355   PGO2 (0.21 g/L) were similar but that of TFC–PGO4 (0.15 g/L) was much lower, possibly due to

356   the additional resistance from nonporous GO flakes. The TFC–PGO2 was chosen as the optimal

357   membrane as it showed the highest water flux among the other modified TFC membranes without

358   affecting the membrane selectivity. Moreover, the enhanced selectivity of the modified membranes

359   makes them promising for application in wastewater reclamation and desalination.

360   The intrinsic transport properties of the pristine and modified TFC membranes examined

361   in this work were evaluated from the pure water permeability coefficient (A) and solute

362   permeability coefficient (B), which are listed in Table 2. The modified membranes demonstrated

363   lower A and B values than the pristine TFC membrane (6.41 $L.m^{-2}.h^{-1}.bar^{-1}$ and 1.15 $L.m^{-2}.h^{-1}$,

364   respectively). The additional dense PVA or PVA/GO hydrogel layer on the TFC membrane surface

365   lessened the permeability and increased the selectivity of the modified membranes by increasing

366   the hydraulic resistance across the membrane. The modified membranes TFC–PGO1 (3.98 $L.m^{-2}.h^{-1}.bar^{-1}$)

367    $^{2}.h^{-1}.bar^{-1}$) and TFC–PGO2 (4.75 $L.m^{-2}.h^{-1}.bar^{-1}$) demonstrated higher A values than the TFC–P

368   (3.41 $L.m^{-2}.h^{-1}.bar^{-1}$) membrane due to their enhanced hydrophilicity and less dense PVA/GO

369   layer resulting from the uneven hydrogel coating. The TFC–PGO4; however, exhibited the lowest

370   A value (2.97 $L.m^{-2}.h^{-1}.bar^{-1}$) due to the formation of a very dense, tortuous and partially

371   nonporous PVA/GO hydrogel layer coating. The dense hydrogel layers reduced the B values of

372   the modified membranes than the pristine TFC membrane through the size exclusion effect. The

373   intrinsic membrane selectivity ratio (B/A) is shown in Table 2, where a more selective membrane

374   is represented by a smaller B/A ratio and vice versa. The pristine TFC membrane revealed the

375   largest B/A ratio of 0.18 bar; while TFC–PGO4 revealed the highest selectivity with the lowest

19

376 B/A ratio of 0.04 bar. The intrinsic transport parameters of the membranes are in good conformity

377 with the FO test results shown in **Fig. 5**, and demonstrated that their separation performance could

378 be tuned by simply adjusting the GO loading in the PVA hydrogel coating. Moreover, the

379 improved selectivity of the modified membranes suggests that the PVA hydrogel coating could be

380 used to seal defects on the PA TFC membrane.

381 **3.3 Membrane fouling study**

382   The antifouling properties of the pristine and hydrogel-coated TFC membranes were

383 assessed from the FO fouling tests with the membranes placed in AL-FS orientation. The TFC,

384 TFC–P and TFC–PGO2 were utilised to study the influence of PVA hydrogel and GO flakes on

385 the fouling tendency of the TFC membranes. Fig. 6 presents the normalised membrane water flux

386 ($J_w/J_{w,0}$) obtained throughout the fouling experiment. The initial water flux ($J_{w,0}$) for all the

387 membranes was set to ~22 L.m^{-2}.h^{-1}. Baseline tests were conducted for 1 h with foulant-free FS

388 that resulted in stable water flux through the membranes (Fig. 6a). The normalised water flux for

389 the membranes immediately declined after foulants were added to the FS as they experienced

390 increased transport resistance from foulant buildup on their surfaces, which eventually hindered

391 water permeability across the membranes (Fig. 6b). Despite possessing the most negatively

392 charged surface (**Fig. 4**b), the pristine TFC membrane failed to repel the negatively charged

393 alginate molecules effectively and experienced the maximum flux decline at the end of the fouling

394 study, which reached a normalised flux of 0.35. The observed fouling behaviour can be attributed

395 to the bridging effects of the calcium ions between the PA layer and the alginate chains to form a

396 gel-like alginate layer on the TFC membrane surface [44, 45]. Besides, the comparatively rougher

397 and less hydrophilic surface of the pristine TFC membrane promoted more foulant adhesion on its

20

398   surface than the modified TFC–P and TFC–PGO2 membranes. Moreover, the relatively poor

399   selectivity of the TFC membrane could have accelerated its fouling from the existence of

400   electrostatic attraction amid the DS ions and the charged foulants [17].

401   The modified membranes, on the other hand, showed significantly better antifouling

402   properties than the pristine TFC membrane with the TFC–PGO2 exhibiting the lowest flux decline

403   (Fig. 6b). The TFC–P and TFC–PGO2 membranes reached normalised fluxes of 0.69 and 0.81,

404   respectively, at the end of the 5 h fouling test. The improved antifouling properties of the modified

405   membranes could be attributed to their smooth surfaces that restrained the attachment of

406   hydrophobic foulant on their surfaces by offering lesser adhesion sites. The hydrophilic modified

407   membranes prevented the attachment of hydrophobic alginate molecules by forming a layer of

408   hydrogen-bonded water molecules on their surfaces [46]. The better fouling resistance of the TFC–

409   PGO2 membrane than the TFC–P membrane could be attributed to its improved hydrophilicity.

410   After finishing the fouling tests, the membranes were rinsed physically with DI water for 1

411   h and tested under baseline conditions to determine their flux recovery. As can be seen from **Fig.**

412   **6**c, the normalised flux increased for the membranes following the cleaning procedure, which

413   signifies that the membranes demonstrated reversible fouling to a certain degree. The pristine TFC

414   membrane achieved a low flux recovery of 62%; thus, showing significant irreversible fouling due

415   to strong fouling layer adhesion on the membrane surface. In contrast, the modified TFC–P and

416   TFC–PGO2 membranes demonstrated comparatively high flux recoveries of 99% and 98%,

417   respectively, which can be associated to their smoother surfaces that allowed simpler foulant

418   removal owing to the existence of less foulant adhesive sites on their surfaces. Moreover, the

419   improved hydrophilicity of the TFC–P and TFC–PGO2 membranes diminished the interaction

21

420   between foulant and their surfaces that led to the development of a loosely bound foulant layer that

421   could be removed effortlessly using a high cross-flow velocity in the cleaning stage. Hence, it can

422   be established from the fouling results that the fouling was partially reversible by physical cleaning

423   for the pristine TFC membrane but almost completely reversible for the TFC–P and TFC–PGO2

424   membranes.

425   **3.4   Membrane foulant resistance**

426   The transient foulant resistances (R_f) of the pristine TFC, TFC–P and TFC–PGO2

427   membranes were established from the osmotic-resistance filtration models using the

428   experimentally determined membrane resistance (R_m) (Table S2), structural parameter of 409 µm,

429   water flux and osmotic driving force. The water flux was obtained from the FO fouling experiment,

430   as shown in Fig. 6. The R_f for pristine TFC membrane increased more rapidly as the fouling

431   progressed than that for the modified membranes (Fig. 7). At the end of the fouling test, the R_f for

432   TFC membrane (4.89×10^{14} m^{-1}) was over 3.5 and 8.7 times greater than that for TFC–P

433   (1.38×10^{14} m^{-1}) and TFC–PGO2 (0.56×10^{14} m^{-1}) membranes, respectively. The comparison of

434   foulant resistances demonstrate that the pristine TFC membrane is the most susceptible to foulant

435   deposition, whereas the GO-incorporated TFC–PGO2 membrane is the least prone to fouling.

436   **3.5   Bacterial anti-adhesion performance**

437   The anti-biofouling performance of the membrane samples was examined via static bacterial

438   adhesion tests using *Bacillus subtilis* as the model bacteria. **Fig. 8** shows the epifluorescent images

439   of *Bacillus subtilis* biofilms on the control pristine TFC membrane and the modified TFC

440   membranes. After 24 h exposure to the bacterial solution, the pristine TFC membrane showed

441   maximum bacterial adhesion (Fig. 8a). The bacterial adhesion on the modified membranes were

442   normalised with that on the pristine TFC membrane. The modified TFC membranes (Fig. 8b-e)

443   showed substantially lower relative bacterial coverage than the pristine TFC membrane as they

444   possess smoother and more hydrophilic surface than the pristine TFC membrane. The smoother

445   surfaces of the modified membranes provided fewer sites for bacterial adhesion. While, the

446   improved membrane surface hydrophilicity weakened the adsorption of hydrophobic bacteria to

447   the surface by creating a hydration layer on the membrane surface [47].

448   The PVA/GO-coated TFC membranes exhibited superior antibacterial activity compared to

449   the TFC and TFC–P membranes, and the relative bacterial coverage on the PVA/GO-coated TFC

450   membranes decreased with increasing GO loading (Fig. 8c-e). The relative bacterial adhesion of

451   the PVA/GO-modified membrane decreased from 27% to 9% when the GO loading was increased

452   from 0.01 wt% to 0.04%, which proves the biocidal effect of PVA/GO coating (**Fig. 9**). In addition

453   to the membrane hydrophilicity, the enhanced antibacterial properties of the PVA/GO-modified

454   membranes could be attributed to their negatively charged membrane surfaces and the biocidal

455   effect of the exposed GO flakes [27]. The more negatively-charged surface of the PVA/GO-

456   modified membranes arising from the epoxide, hydroxyl and carboxyl groups of the GO flakes

457   could mitigate bacterial adhesion on their surfaces by electrostatically repelling the negatively-

458   charged bacteria and extracellular polymeric substance, which is closely associated to biofilm

459   development [48]. The biocidal activity of the exposed GO flakes is associated to their reactive

460   edges that damage bacterial cell by creating oxidative stress or rupturing the cell membrane;

461   thereby, leading to viability loss and death of bacterial cell [49]. The results suggest that addition

462   on GO in PVA hydrogel can effectively suppress the bacterial adhesion and growth on the

463 membrane surface, thereby, considerably augmenting the anti-biofouling property of the
464 membranes.

4 Conclusions

466 Commercial PA TFC FO membranes were coated with a thin layer of cross-linked PVA and
467 PVA/GO hydrogel to increase the selectivity, antifouling and anti-biofouling properties of the
468 membranes. The hydrogel coating smoothened and improved the wettability of the membrane
469 surface, while slightly declining the water flux. The membrane surface properties, performances
470 and antibacterial properties were tuned by adjusting the GO loading in the PVA hydrogel coating.
471 Modified TFC membrane with a GO loading of 0.02 wt% (TFC–PGO2) is chosen as the optimal
472 membrane as it revealed the highest water flux amongst the modified membranes without
473 sacrificing membrane selectivity. The TFC–PGO2 membrane exhibited improved solute rejection,
474 cleaning efficiency and bacterial resistance with a 55% lower SRSF, 36% higher flux recovery and
475 82% lower relative bacterial coverage compared to the pristine TFC membrane. Consequently, the
476 facile PVA/GO modification technique demonstrated in this study could be used to effectively seal
477 the membrane defects and improve antifouling and anti-biofouling performance for potential
478 application in wastewater reclamation and desalination.

CRediT authorship contribution statement

480 **Nawshad Akther:** Conceptualisation, Data curation, Formal analysis, Investigation,
481 Methodology, Validation, Writing - original draft. **Syed Muztuza Ali:** Methodology, Formal
482 analysis. **Sherub Phuntsho:** Writing - review & editing, Funding acquisition,

483   Supervision. **Hokyong Shon:** Supervision, Project administration, Resources, Funding

484   acquisition, Validation, Writing - review & editing.

Acknowledgement

490

491

492 **Figures**

493 **Table 1:** Surface modification conditions of PA TFC FO membranes.

494 **Fig. 1:** ATR-FTIR spectra of the pristine and modified TFC membranes.

495 **Fig. 2:** SEM images revealing the surface morphology of the (a) pristine TFC membrane; and PVA
496 hydrogel coated TFC membranes with different GO loadings: (b) 0, (c) 0.01, (d) 0.02, and (e) 0.04
497 wt%.

498 **Fig. 3:** AFM images revealing the surface roughness of the (a) pristine TFC membrane; and PVA
499 hydrogel coated TFC membranes with different GO loadings: (b) 0, (c) 0.01, (d) 0.02, and (e) 0.04
500 wt%. Error bars for membrane surface roughness represent one standard error obtained from at
501 least four membrane samples for each condition.

502 **Fig. 4:** (a) Water contact angle measurements, and (b) zeta potentials as a function of pH for the
503 pristine and modified TFC membrane surfaces. Error bars for water contact angle measurements
504 represent one standard error obtained from at least seven measurements for each membrane sample.

505 **Fig. 5:** FO performance of the pristine and modified TFC membranes. Operating conditions: FS,
506 DI water; DS, 1 M NaCl; cross-flow velocity, 12.6 cm/s; membrane orientation, AL-FS. Error bars
507 represent one standard error obtained from at least three membrane samples for each condition.

508 **Table 2:** Intrinsic transport parameters of the membranes.

509 **Fig. 6:** Normalised flux of the pristine and modified TFC membranes during the FO (a) baseline
510 test, (b) fouling test and (c) after hydraulic cleaning. Operating conditions: Initial baseline water
511 flux ($J_{w,0}$), ~22 L.m^{-2}.h^{-1}; DS, 0.5 M to 1 M NaCl; flow rate (baseline and fouling test), 0.5 L/min;
512 flow rate (physical cleaning), 0.7 L/min; membrane orientation, AL-FS; foulants, 1 mM calcium
513 chloride and 200 ppm SA.

514 **Fig. 7:** Foulant resistance of pristine and modified TFC membranes during the FO fouling test.

515 **Fig. 8:** Static bacterial adhesion on (a) pristine and modified TFC membranes with different GO
516 loadings: (b) 0, (c) 0.01, (d) 0.02, and (e) 0.04 wt%.

517 **Fig. 9:** Relative bacterial coverage on the pristine and modified TFC membrane surfaces. The
518 bacterial adhesion on each membrane surface was normalised with respect to the pristine TFC
519 membrane. Error bars represent one standard error obtained from at least three membrane samples
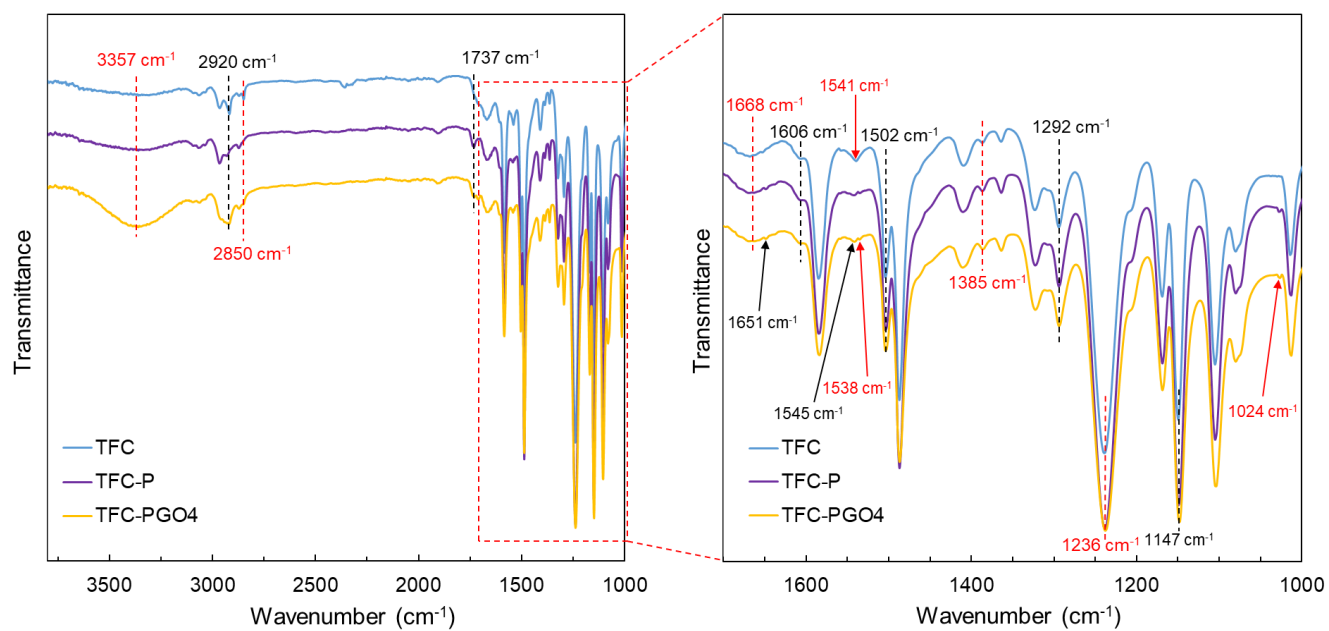520 for each condition.

521

522

Table 3

Membrane	PVA (wt%)	GO (wt/v%)
TFC	0	0
TFC–P	0.25	0
TFC–PGO1	0.25	0.01
TFC–PGO2	0.25	0.02
TFC–PGO4	0.25	0.04

523

524

525

Fig. 10

TFC

TFC–P

TFC–PGO1

a

1 µm

500 nm

b

1 µm

500 nm

c

1 µm

500 nm

TFC–PGO2

TFC–PGO4

d

1 µm

500 nm

e

1 µm

500 nm

526

527   Fig. 11

528

TFC

$R_q = 42.0 \pm 1.9$ nm

TFC–P

$R_q = 29.8 \pm 2.7$ nm

TFC–PGO1

$R_q = 38.0 \pm 1.2$ nm

TFC–PGO2

$R_q = 34.2 \pm 1.9$ nm

TFC–PGO4

$R_q = 28.8 \pm 2.2$ nm

529

530   Fig. 12

531

532

533   Fig. 13

534

535

Fig. 14

536

537
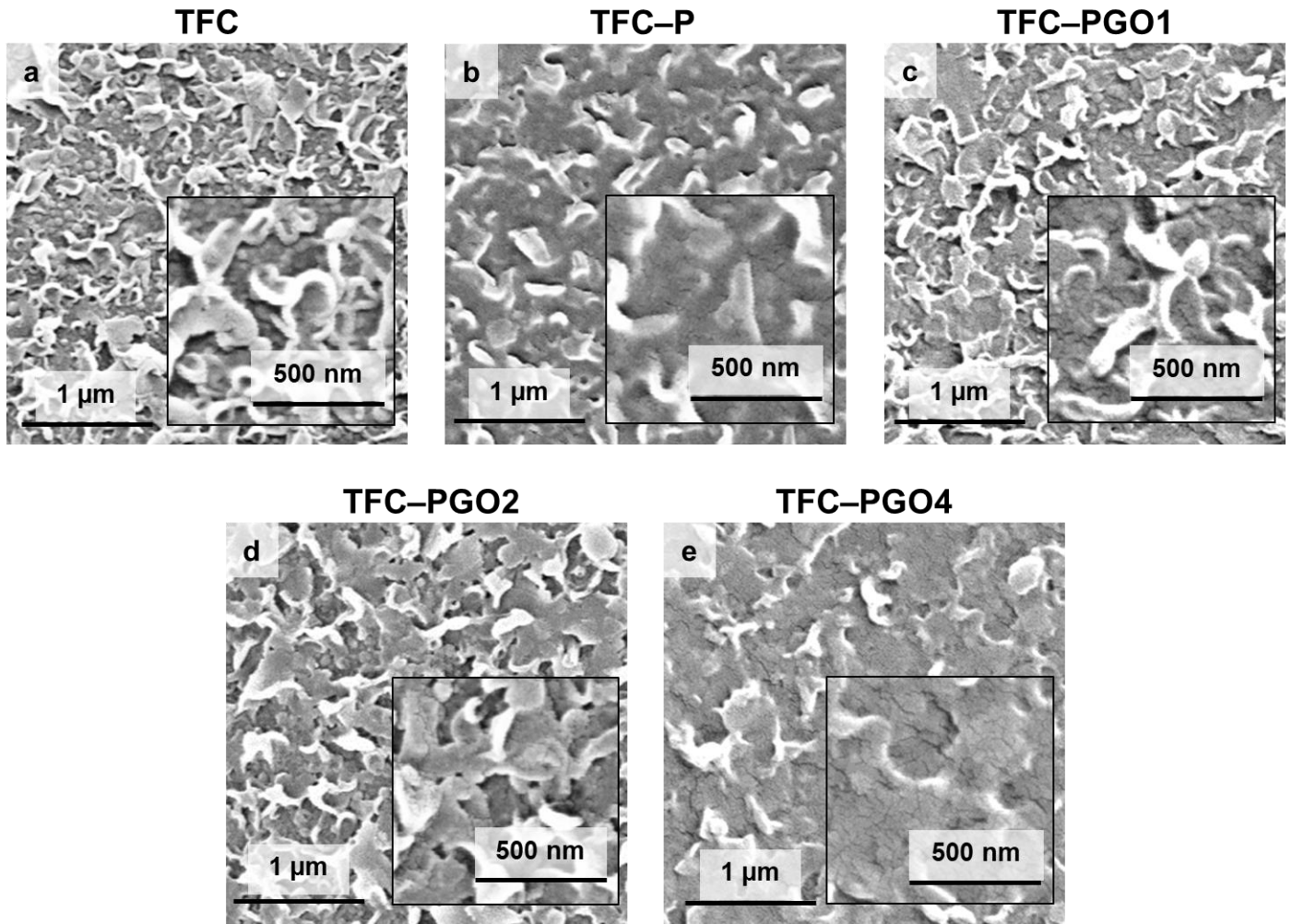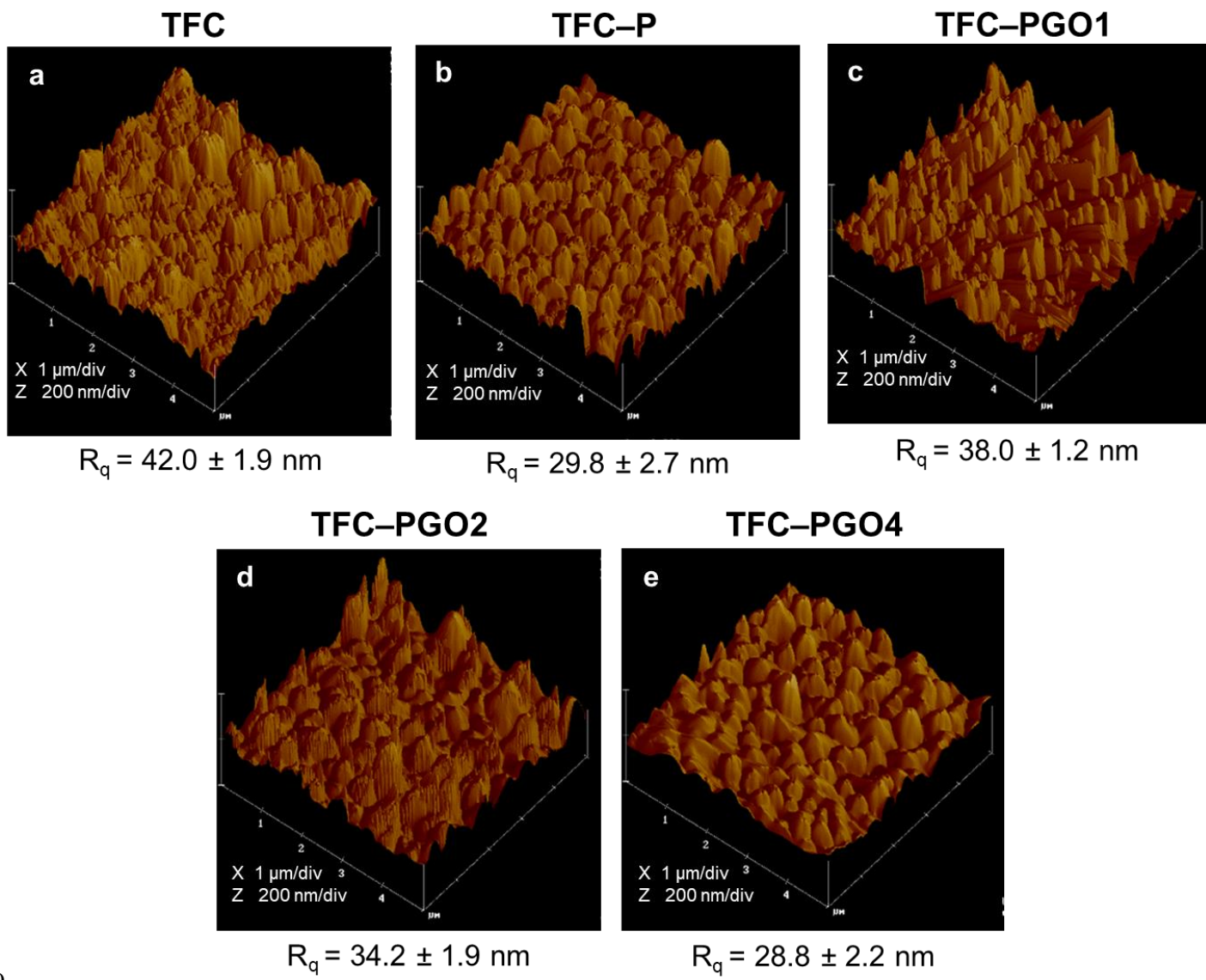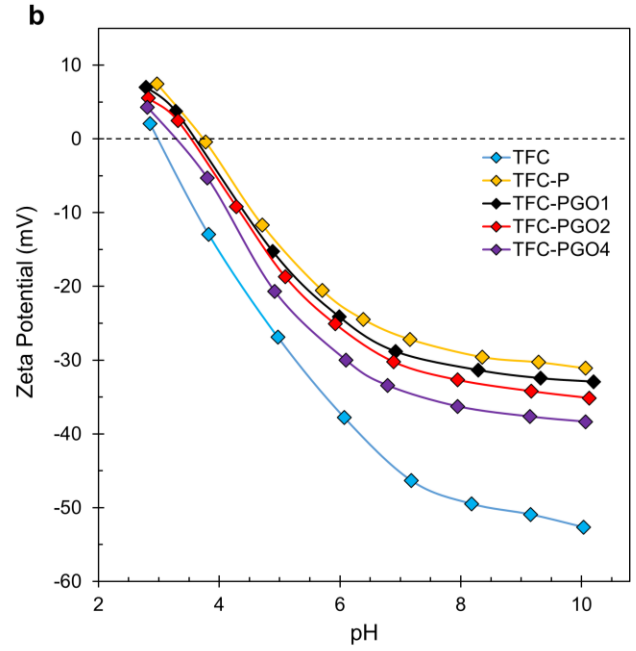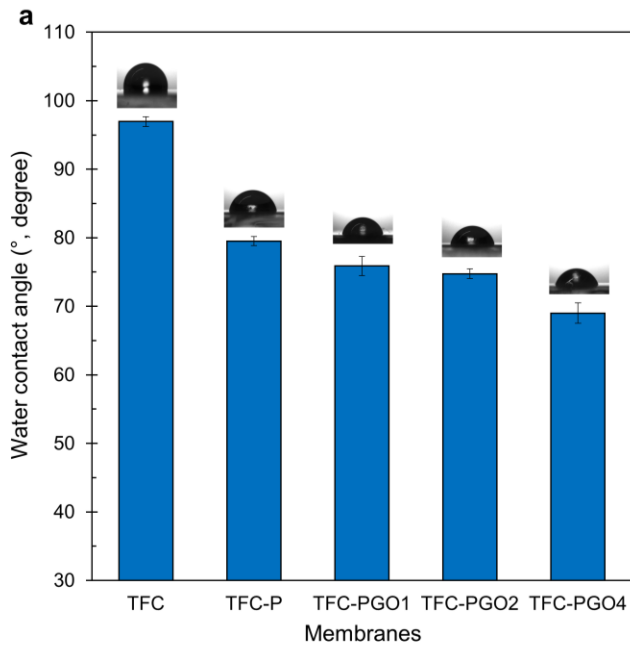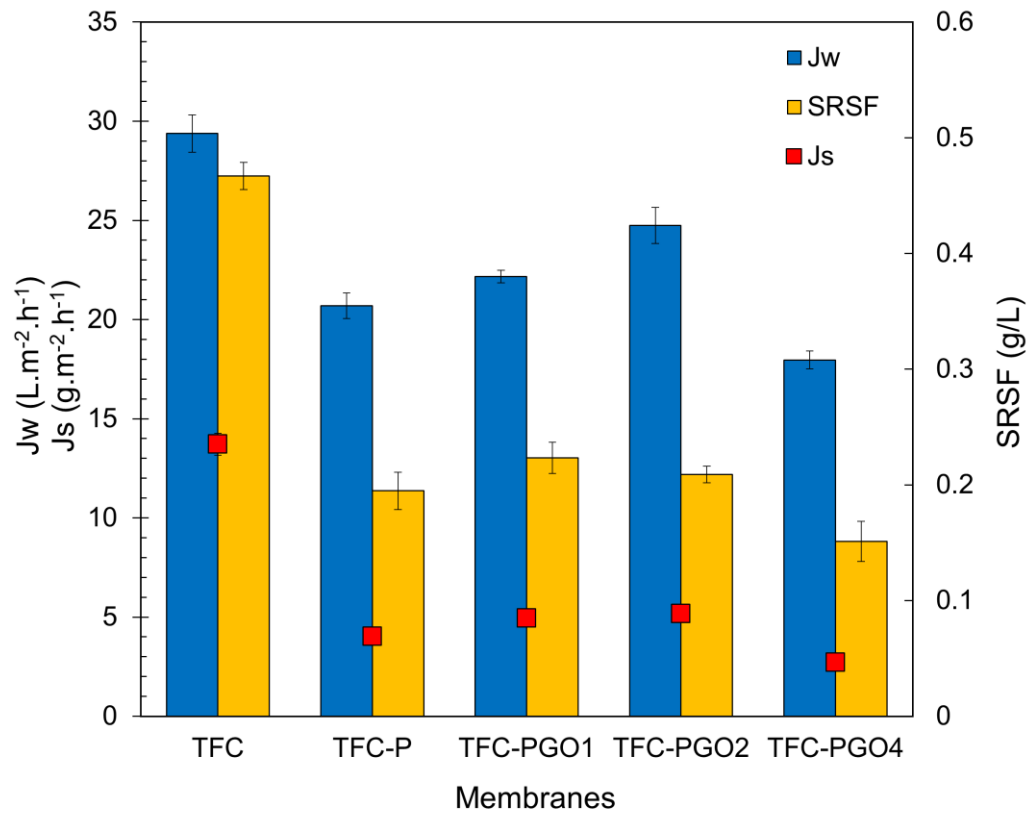
538

Table 4

Membrane	A (L.m^{-2}.h^{-1}.bar^{-1})	B (L.m^{-2}.h^{-1})	B/A (bar)
TFC	6.41	1.15	0.18
TFC–P	3.41	0.22	0.06
TFC–PGO1	3.98	0.30	0.08
TFC–PGO2	4.75	0.31	0.07
TFC–PGO4	2.97	0.12	0.04

539
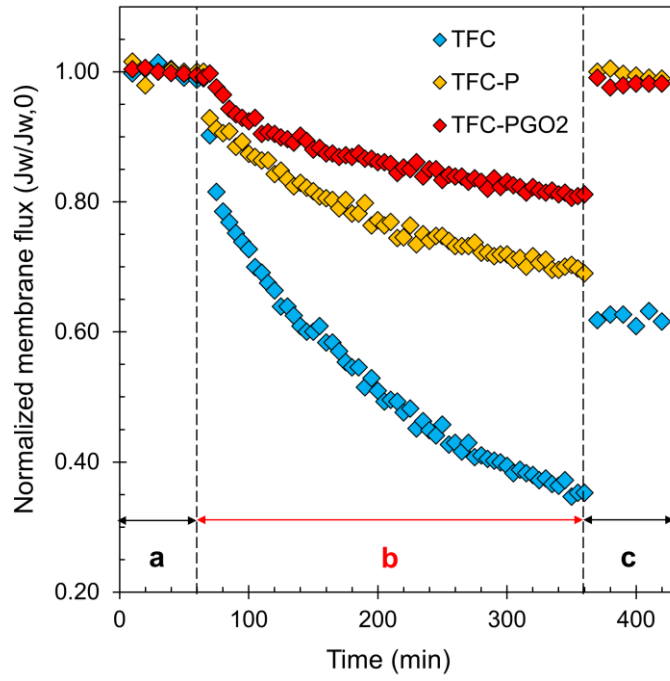
540

541   Fig. 15
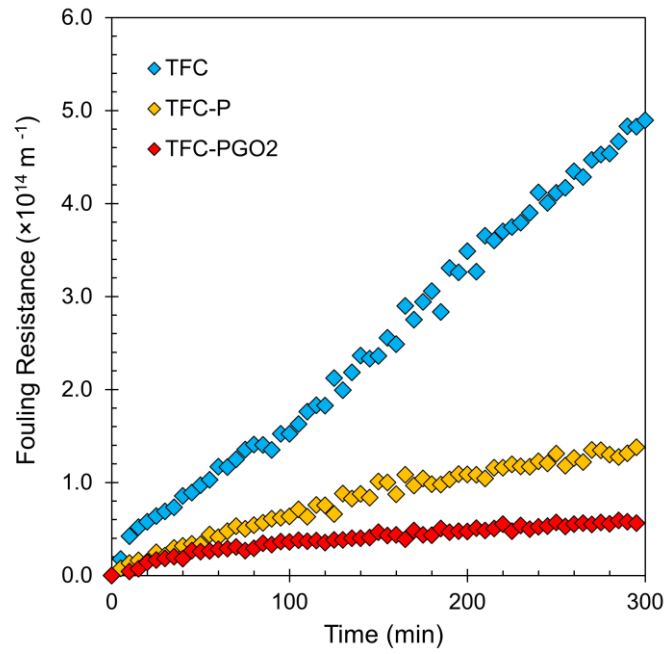
542

543   Fig. 16

TFC   **TFC–P**   **TFC–PGO1**   **TFC–PGO2**   **TFC–PGO4**

544

545   Fig. 17
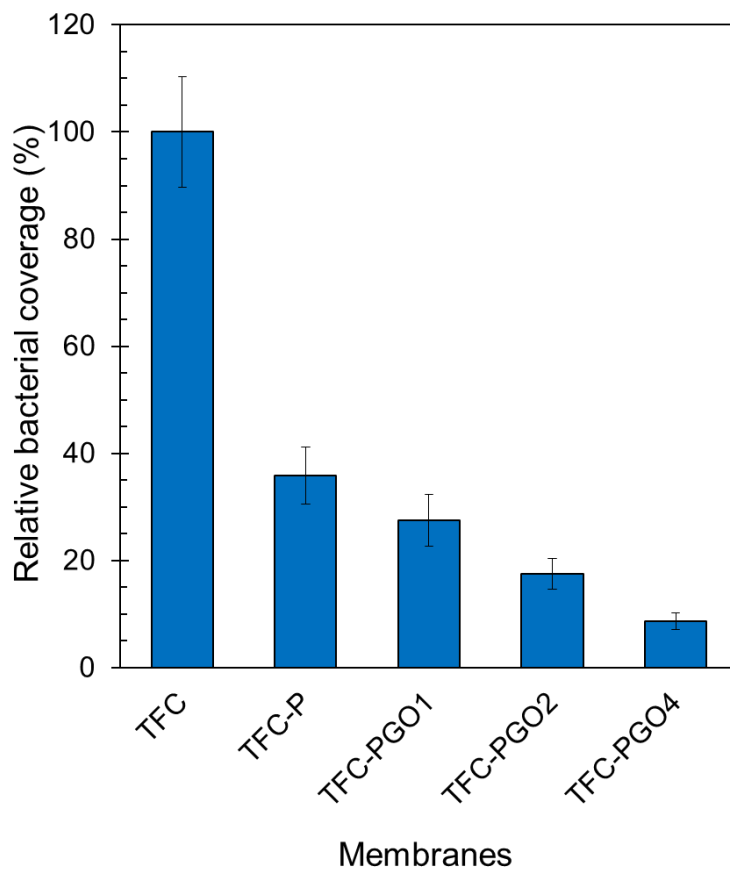
546

547

548   Fig. 18

549

550

551
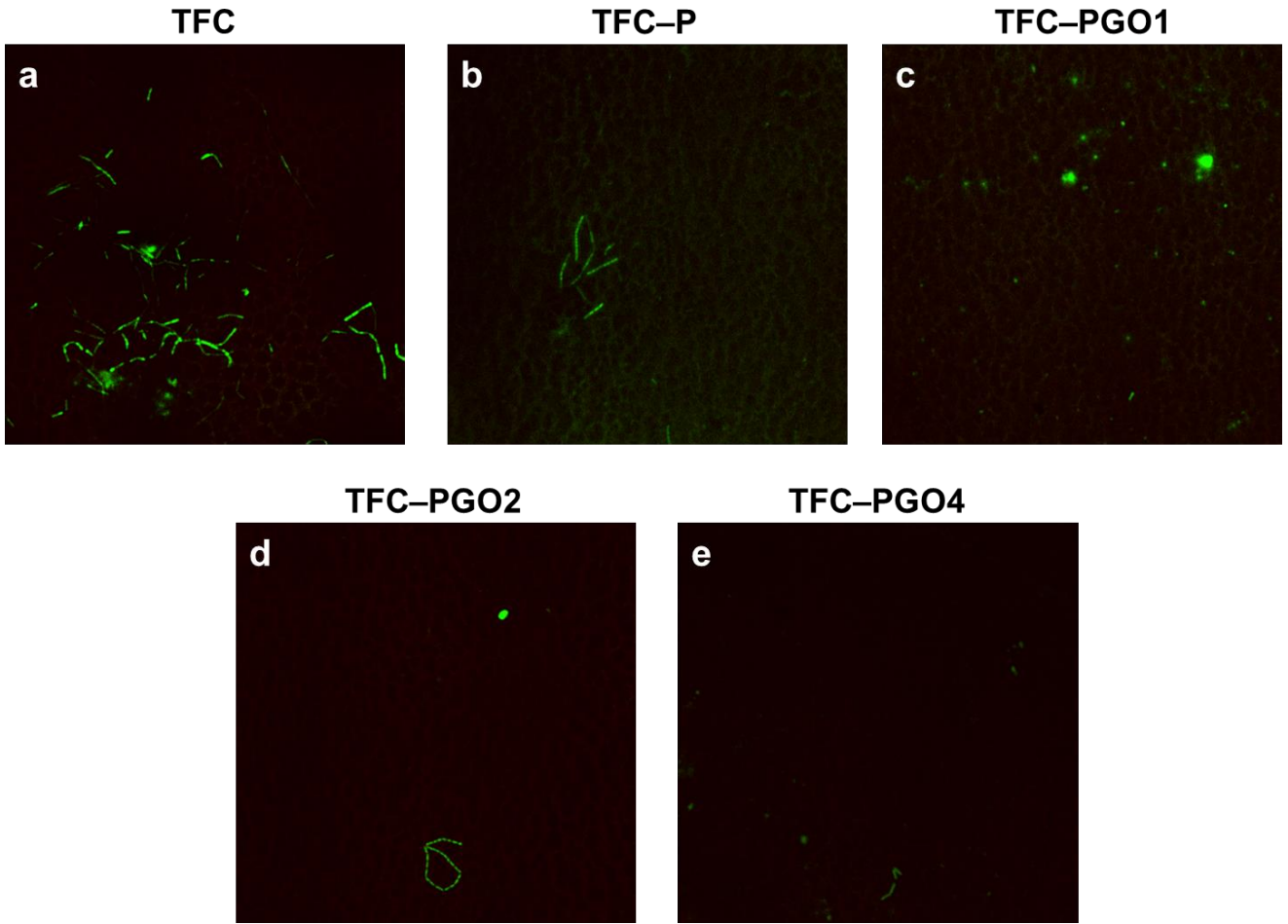
References

[1] M.A. Shannon, P.W. Bohn, M. Elimelech, J.G. Georgiadis, B.J. Mariñas, A.M. Mayes, Science and technology for water purification in the coming decades, Nature, 452 (2008) 301-310.

[2] I.C. Kim, Y.H. Ka, J.Y. Park, K.H. Lee, Preparation of fouling resistant nanofiltration and reverse osmosis membranes and their use for dyeing wastewater effluent, J. Ind. Eng. Chem., 10 (2004) 115-121.

[3] S. Mozia, Photocatalytic membrane reactors (PMRs) in water and wastewater treatment. A review, Separation and Purification Technology, 73 (2010) 71-91.

[4] L. Chen, Y. Gu, C. Cao, J. Zhang, J.-W. Ng, C. Tang, Performance of a submerged anaerobic membrane bioreactor with forward osmosis membrane for low-strength wastewater treatment, Water Research, 50 (2014) 114-123.

[5] S.M. Ali, J.E. Kim, S. Phuntsho, A. Jang, J.Y. Choi, H.K. Shon, Forward osmosis system analysis for optimum design and operating conditions, Water Research, 145 (2018) 429-441.

[6] N. Akther, A. Sodiq, A. Giwa, S. Daer, H.A. Arafat, S.W. Hasan, Recent advancements in forward osmosis desalination: A review, Chemical Engineering Journal, 281 (2015) 502-522.

[7] B. Mi, M. Elimelech, Organic fouling of forward osmosis membranes: Fouling reversibility and cleaning without chemical reagents, Journal of Membrane Science, 348 (2010) 337-345.

[8] N. Akther, S. Daer, Q. Wei, I. Janajreh, S.W. Hasan, Synthesis of polybenzimidazole (PBI) forward osmosis (FO) membrane and computational fluid dynamics (CFD) modeling of concentration gradient across membrane surface, Desalination, 452 (2019) 17-28.

[9] V.H. Tran, S. Lim, D.S. Han, N. Pathak, N. Akther, S. Phuntsho, H. Park, H.K. Shon, Efficient fouling control using outer-selective hollow fiber thin-film composite membranes for osmotic membrane bioreactor applications, Bioresource Technology, 282 (2019) 9-17.

[10] J.E. Kim, J. Kuntz, A. Jang, I.S. Kim, J.Y. Choi, S. Phuntsho, H.K. Shon, Techno-economic assessment of fertiliser drawn forward osmosis process for greenwall plants from urban wastewater, Process Safety and Environmental Protection, 127 (2019) 180-188.

[11] H. Zhu, L. Zhang, X. Wen, X. Huang, Feasibility of applying forward osmosis to the simultaneous thickening, digestion, and direct dewatering of waste activated sludge, Bioresource Technology, 113 (2012) 207-213.

[12] K.B. Petrotos, H.N. Lazarides, Osmotic concentration of liquid foods, Journal of Food Engineering, 49 (2001) 201-206.

[13] K. Lutchmiah, A.R.D. Verliefde, K. Roest, L.C. Rietveld, E.R. Cornelissen, Forward osmosis for application in wastewater treatment: A review, Water Research, 58 (2014) 179-197.

[14] N. Akther, S. Daer, S.W. Hasan, Effect of flow rate, draw solution concentration and temperature on the performance of TFC FO membrane, and the potential use of RO reject brine as a draw solution in FO–RO hybrid systems, Desalination and Water Treatment, 136 (2018) 65-71.

[15] Q.V. Ly, Y. Hu, J. Li, J. Cho, J. Hur, Characteristics and influencing factors of organic fouling in forward osmosis operation for wastewater applications: A comprehensive review, Environment International, 129 (2019) 164-184.

[16] N. Akther, S. Lim, V.H. Tran, S. Phuntsho, Y. Yang, T.-H. Bae, N. Ghaffour, H.K. Shon, The effect of Schiff base network on the separation performance of thin film nanocomposite forward osmosis membranes, Separation and Purification Technology, 217 (2019) 284-293.

594   [17] S. Lim, V.H. Tran, N. Akther, S. Phuntsho, H.K. Shon, Defect-free outer-selective hollow
595   fiber thin-film composite membranes for forward osmosis applications, Journal of Membrane
596   Science, 586 (2019) 281-291.
597   [18] D. Emadzadeh, W.J. Lau, T. Matsuura, N. Hilal, A.F. Ismail, The potential of thin film
598   nanocomposite membrane in reducing organic fouling in forward osmosis process, Desalination,
599   348 (2014) 82-88.
600   [19] N. Akther, S. Phuntsho, Y. Chen, N. Ghaffour, H.K. Shon, Recent advances in nanomaterial-
601   modified polyamide thin-film composite membranes for forward osmosis processes, Journal of
602   Membrane Science, 584 (2019) 20-45.
603   [20] S. Lim, N. Akther, V.H. Tran, T.-H. Bae, S. Phuntsho, A. Merenda, L.F. Dumée, H.K. Shon,
604   Covalent organic framework incorporated outer-selective hollow fiber thin-film nanocomposite
605   membranes for osmotically driven desalination, Desalination, 485 (2020) 114461.
606   [21] S. Lim, K.H. Park, V.H. Tran, N. Akther, S. Phuntsho, J.Y. Choi, H.K. Shon, Size-controlled
607   graphene oxide for highly permeable and fouling-resistant outer-selective hollow fiber thin-film
608   composite membranes for forward osmosis, Journal of Membrane Science, (2020) 118171.
609   [22] M. Liu, Q. Chen, L. Wang, S. Yu, C. Gao, Improving fouling resistance and chlorine stability
610   of aromatic polyamide thin-film composite RO membrane by surface grafting of polyvinyl alcohol
611   (PVA), Desalination, 367 (2015) 11-20.
612   [23] Q. Zhang, C. Zhang, J. Xu, Y. Nie, S. Li, S. Zhang, Effect of poly(vinyl alcohol) coating
613   process conditions on the properties and performance of polyamide reverse osmosis membranes,
614   Desalination, 379 (2016) 42-52.
615   [24] A. Giwa, N. Akther, V. Dufour, S.W. Hasan, A critical review on recent polymeric and nano-
616   enhanced membranes for reverse osmosis, RSC Advances, 6 (2016) 8134-8163.
617   [25] A. Inurria, P. Cay-Durgun, D. Rice, H. Zhang, D.-K. Seo, M.L. Lind, F. Perreault, Polyamide
618   thin-film nanocomposite membranes with graphene oxide nanosheets: Balancing membrane
619   performance and fouling propensity, Desalination, 451 (2018) 139-147.
620   [26] Y. Qian, X. Zhang, C. Liu, C. Zhou, A. Huang, Tuning interlayer spacing of graphene oxide
621   membranes with enhanced desalination performance, Desalination, 460 (2019) 56-63.
622   [27] H.M. Hegab, A. ElMekawy, T.G. Barclay, A. Michelmore, L. Zou, C.P. Saint, M. Ginic-
623   Markovic, Effective in-situ chemical surface modification of forward osmosis membranes with
624   polydopamine-induced graphene oxide for biofouling mitigation, Desalination, 385 (2016) 126-
625   137.
626   [28] J. Yin, G. Zhu, B. Deng, Graphene oxide (GO) enhanced polyamide (PA) thin-film
627   nanocomposite (TFN) membrane for water purification, Desalination, 379 (2016) 93-101.
628   [29] F. Peng, Z. Jiang, E.M.V. Hoek, Tuning the molecular structure, separation performance and
629   interfacial properties of poly(vinyl alcohol)–polysulfone interfacial composite membranes,
630   Journal of Membrane Science, 368 (2011) 26-33.
631   [30] N. Akther, Z. Yuan, Y. Chen, S. Lim, S. Phuntsho, N. Ghaffour, H. Matsuyama, H. Shon,
632   Influence of graphene oxide lateral size on the properties and performances of forward osmosis
633   membrane, Desalination, 484 (2020).
634   [31] A. Tiraferri, N.Y. Yip, A.P. Straub, S. Romero-Vargas Castrillon, M. Elimelech, A method
635   for the simultaneous determination of transport and structural parameters of forward osmosis
636   membranes, Journal of Membrane Science, 444 (2013) 523-538.
637   [32] F.A. Siddiqui, Q. She, A.G. Fane, R.W. Field, Exploring the differences between forward
638   osmosis and reverse osmosis fouling, Journal of Membrane Science, 565 (2018) 241-253.

639 [33] G.S. Lai, W.J. Lau, P.S. Goh, A.F. Ismail, Y.H. Tan, C.Y. Chong, R. Krause-Rehberg, S.
640 Awad, Tailor-made thin film nanocomposite membrane incorporated with graphene oxide using
641 novel interfacial polymerization technique for enhanced water separation, Chemical Engineering
642 Journal, 344 (2018) 524-534.
643 [34] C.Y. Tang, Y.-N. Kwon, J.O. Leckie, Effect of membrane chemistry and coating layer on
644 physiochemical properties of thin film composite polyamide RO and NF membranes: I. FTIR and
645 XPS characterization of polyamide and coating layer chemistry, Desalination, 242 (2009) 149-167.
646 [35] Y. Hu, K. Lu, F. Yan, Y. Shi, P. Yu, S. Yu, S. Li, C. Gao, Enhancing the performance of
647 aromatic polyamide reverse osmosis membrane by surface modification via covalent attachment
648 of polyvinyl alcohol (PVA), Journal of Membrane Science, 501 (2016) 209-219.
649 [36] G.M. Nisola, L.A. Limjuco, E.L. Vivas, C.P. Lawagon, M.J. Park, H.K. Shon, N. Mittal, I.W.
650 Nah, H. Kim, W.-J. Chung, Macroporous flexible polyvinyl alcohol lithium adsorbent foam
651 composite prepared via surfactant blending and cryo-desiccation, Chemical Engineering Journal,
652 280 (2015) 536-548.
653 [37] H.S. Mansur, C.M. Sadahira, A.N. Souza, A.A.P. Mansur, FTIR spectroscopy
654 characterization of poly (vinyl alcohol) hydrogel with different hydrolysis degree and chemically
655 crosslinked with glutaraldehyde, Materials Science and Engineering: C, 28 (2008) 539-548.
656 [38] C.Y. Tang, Y.-N. Kwon, J.O. Leckie, Effect of membrane chemistry and coating layer on
657 physiochemical properties of thin film composite polyamide RO and NF membranes: II.
658 Membrane physiochemical properties and their dependence on polyamide and coating layers,
659 Desalination, 242 (2009) 168-182.
660 [39] M. Rastgar, A. Shakeri, A. Bozorg, H. Salehi, V. Saadattalab, Highly-efficient forward
661 osmosis membrane tailored by magnetically responsive graphene oxide/Fe3O4 nanohybrid,
662 Applied Surface Science, 441 (2018) 923-935.
663 [40] W.J. Lau, A.F. Ismail, P.S. Goh, N. Hilal, B.S. Ooi, Characterization methods of thin film
664 composite nanofiltration membranes, Separation & Purification Reviews, 44 (2015) 135-156.
665 [41] A.M. Dimiev, L.B. Alemany, J.M. Tour, Graphene Oxide. Origin of Acidity, Its Instability in
666 Water, and a New Dynamic Structural Model, ACS Nano, 7 (2013) 576-588.
667 [42] C. Yu, B. Zhang, F. Yan, J. Zhao, J. Li, L. Li, J. Li, Engineering nano-porous graphene oxide
668 by hydroxyl radicals, Carbon, 105 (2016) 291-296.
669 [43] J.Y. Chong, B. Wang, K. Li, Graphene oxide membranes in fluid separations, Current Opinion
670 in Chemical Engineering, 12 (2016) 98-105.
671 [44] M. Hu, S. Zheng, B. Mi, Organic fouling of graphene oxide membranes and its implications
672 for membrane fouling control in engineered osmosis, Environmental Science & Technology, 50
673 (2016) 685-693.
674 [45] S.I. Yadav, Ibrar; Bakly, Salam; Khanafer, Daoud; Altaee, Ali; Padmanaban, V. C.; Samal,
675 Akshaya K.; Hawari, Alaa H., Organic Fouling in Forward Osmosis: A Comprehensive Review,
676 Water, 12 (2020) 1505.
677 [46] A. Tiraferri, Y. Kang, E.P. Giannelis, M. Elimelech, Superhydrophilic thin-film composite
678 forward osmosis membranes for organic fouling control: Fouling behavior and antifouling
679 mechanisms, Environmental Science & Technology, 46 (2012) 11135-11144.
680 [47] F. Perreault, H. Jaramillo, M. Xie, M. Ude, L.D. Nghiem, M. Elimelech, Biofouling mitigation
681 in forward osmosis using graphene oxide functionalized thin-film composite membranes,
682 Environmental Science & Technology, 50 (2016) 5840-5848.

683   [48] J.W. Costerton, Z. Lewandowski, D.E. Caldwell, D.R. Korber, H.M. Lappin-Scott, Microbial
684   biofilms, Annual Review of Microbiology, 49 (1995) 711-745.
685   [49] W. Hu, C. Peng, W. Luo, M. Lv, X. Li, D. Li, Q. Huang, C. Fan, Graphene-based antibacterial
686   paper, ACS Nano, 4 (2010) 4317-4323.

687